ISSN 1674-1056
http://cpb.iphy.ac.cn
http://iopscience.iop.org/cpb
中国物理 B
Chinese Physics
中国物理
Chinese Physics B

High-performance lens antenna using high refractive index metamaterials

Lai-Jun Wang(王来军), Qiao-Hong Chen(陈巧红), Fa-Long Yu(余发龙), Xi Gao(高喜)

Citation:hin. Phys. B . 2018, 27(8): 087802. **doi:** 10.1088/1674-1056/27/8/087802

Journal homepage: http://cpb.iphy.ac.cn; http://iopscience.iop.org/cpb

What follows is a list of articles you may be interested in

Controlling flexural waves in thin plates by using transformation acoustic metamaterials

Xing Chen(陈幸), Li Cai(蔡力), Ji-Hong Wen(温激鸿)

Chin. Phys. B . 2018, 27(5): 057803. **doi:** 10.1088/1674-1056/27/5/057803

Design and theoretical study of a polarization-insensitive multiband terahertz metamaterial bandpass filter

Hai-Peng Li(李海鹏), Wen-Yue Fu(付文悦), Xiao-Peng Shen(沈晓鹏), Kui Han(韩奎), Wei-Hua Wang(王伟华)

Chin. Phys. B . 2017, 26(12): 127801. **doi:** 10.1088/1674-1056/26/12/127801

Guided mode resonance in planar metamaterials consistingof two ring resonators with different sizes

Zhen Yu(俞禛), Hang Che(陈航), Jianjun Liu(刘建军), Xufeng Jing(井绪峰), Xiangjun Li(李向军), Zhi Hong(洪治)

Chin. Phys. B . 2017, 26(7): 077804. **doi:** 10.1088/1674-1056/26/7/077804

Engineering optical gradient force from coupled surface plasmon polariton modes in nanoscale plasmonic waveguides

Jiahui Lu(卢佳慧), Guanghui Wang(王光辉)

Chin. Phys. B . 2016, 25(11): 117804. **doi:** 10.1088/1674-1056/25/11/117804

Effect of size and indium-composition on linear and nonlinear optical absorption of InGaN/GaN lens-shaped quantum dot

Ahmed S Jbara, Zulkafli Othaman, M A Saeed

Chin. Phys. B . 2016, 25(5): 057801. **doi:** 10.1088/1674-1056/25/5/057801

High-performance lens antenna using high refractive index metamaterials*

Lai-Jun Wang(王来军)[1], Qiao-Hong Chen(陈巧红)[1], Fa-Long Yu(余发龙)[1], and Xi Gao(高喜)[1,2,†]

[1] School of Information and Communication, Guilin University of Electronic Technology, Guilin 541004, China
[2] Guangxi Key Laboratory of Wireless Wideband Communication & Signal Processing, Guilin 541004, China

(Received 12 December 2017; revised manuscript received 4 May 2018; published online 25 July 2018)

In this paper, a high refractive index metamaterial (HRM), whose element is composed of bilayer square patch (BSP) spaced by a dielectric plate, is proposed. By reducing the thickness of the dielectric plate and the gap between adjacent patches, the BSP can effectively enhance capacitive coupling and simultaneously suppress diamagnetic response, which significantly increases the refractive index of the proposed metamaterial. Furthermore, the high refractive index region is far away from the resonant region of the metamaterial, resulting in broadband. Based on these characteristics of BSP, a gradient refractive index (GRIN) lens with thin thickness ($0.34\lambda_0$, where λ_0 is the wavelength at 5.75 GHz) is designed. By using this lens, we then design a circularly polarized horn antenna with high performance. The measurement results show that the 3-dB axial ratio bandwidth is 34.8% (4.75 GHz$\sim$ 6.75 GHz) and the antenna gain in this frequency range is increased by an average value of 3.4 dB. The proposed method opens up a new avenue to design high-performance antenna.

Keywords: circularly polarized horn antenna, high refractive index, lens, metamaterial.

PACS: 78.67.Pt, 84.40.Ba, 84.90.+a **DOI:** 10.1088/1674-1056/27/8/087802

1. Introduction

Lens antennas have attracted extensive attention for their good radiation performances, such as broadband and high-gain, in microwave and millimeter wave ranges. Usually, the traditional lens is realized by processing dielectric plate with different geometries, such as paraboloid, ellipse, etc., with which it can convert (quasi) spherical waves into (quasi) plane waves and hence improve the directivity of antenna.[1,2] However, the conventional methods make lens have bulky profiles and specific thickness requirements. To overcome these drawbacks, some metamaterial lenses, such as negative index metamaterial lens,[3] phase gradient metasurface,[4,5] Huygens metasurface,[6,7] Transmitarray,[8] and GRIN metamaterial lens,[9–17] have been proposed to manipulate the electromagnetic (EM) waves. For the first four metamaterial lenses, they are usually constructed with resonant elements, so they have obvious disadvantages of narrow bandwidth and large transmission loss. Alternatively, the GRIN metamaterial lens can avoid these drawbacks because it is usually comprised of non-resonant elements. Especially for the lens consisting of HRM, its thickness can be significantly decreased and then reduce the dielectric loss. Recently, many HRMs have been successfully designed in the terahertz regime.[18–21] The quasi-static value of the refractive index can reach to 20. However, so far, there are few studies focusing on applications of HRM in microwave frequency range.

In this paper, we propose a polarization insensitive and broadband HRM that is composed of BSP spaced by a dielectric plate. We show that, by reducing the thickness of the dielectric plate and the gap between adjacent patches, the BSP exhibits strong capacitive coupling and paramagnetic effect, resulting in the enhancement of refractive index of the proposed metamaterial. Furthermore, the frequency region of high refractive index is far away from the resonant frequency of BSP, which makes the metamaterial have a flat value of high refractive index in broadband. Based on the proposed HRM, we further construct a GRIN lens which has the properties of broadband, polarization insensitivity and thin thickness. By using this lens we also design a circular polarized horn antenna. Attributing to the lens placed inside the horn, the size of antenna is effectively reduced while the antenna performance, such as the directivity and the gain, is improved greatly.

2. High refractive index metamaterial design

Figure 1(a) shows the unit cell of the proposed HRM, which is composed of BSP and a dielectric plate. RO4350B ($\varepsilon_{r1} = 3.66$ and $\delta_1 = 0.0037$) with thickness $h_1 = 0.508$ mm is used as the dielectric plate, which is employed to separate the BSP. The patches in BSP have the same geometric parameters ($l = 5.9$ mm and $t_1 = 0.018$ mm) and are symmetrically etched on both sides of the dielectric plate. The periods in the x and y directions are equal and set as $p = 6$ mm. For comparison,

*Project supported by the National Natural Science Foundation of China (Grant Nos. 61761010 and 61461016), in part by the Natural Science Foundation of Guangxi Zhuang Autonomous Region, China (Grant No. 2015jjBB7002), in part by the Guangxi Key Laboratory of Wireless Wideband Communication and Signal Processing, and in part by the Innovation Project of GUET Graduate Education (Grant No. 2018JCX24).

†Corresponding author. E-mail: gao_xi76@163.com

© 2018 Chinese Physical Society and IOP Publishing Ltd

we also study a metamaterial with unit cell consisting of bilayer square ring (BSR), as shown in Fig. 1(b). The width of the metallic strip in BSR is set as $w = 0.1$ mm and the other parameters, such as h_1, l, p, and t_1, are the same as that of BSP.

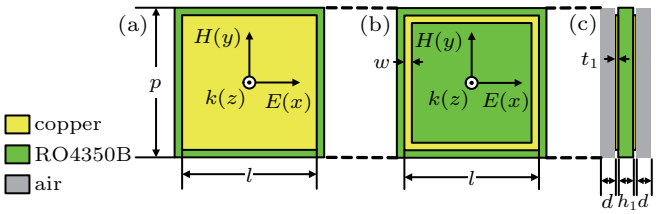


Fig. 1. (color online) Configurations of the proposed metamaterial unit cell: (a) The front view of BSP, (b) the front view of BSR, and (c) side view of both BSP and BSR.

With the help of the commercial software CST Microwave Studio, we first investigate the effective parameters of the two metamaterials. In simulations, a single unit cell with periodic boundary conditions along the x and y directions is employed to simulate the S parameters under the condition of treating physical thickness as effective thickness (i.e. $d = 0$ mm). The unit cell is excited with a normal incident EM wave, as shown in Figs. 1(a) and 1(b). According to Ref. [22], the retrieved effective parameters can be calculated from the simulated S parameters, which are shown in Fig. 2.

From Figs. 2(a) and 2(b), we clearly see that the resonant frequency of BSP is much higher than that of BSR, which makes the effective permittivity (ε_r) and permeability (μ_r) of BSP increase smoothly over a broader frequency range, and hence the BSP metamaterial has a flat refractive index in wideband. Figure 2(c) presents the refractive indices of both metamaterials, from which we observe that the bandwidth of BSP metamaterial with high refractive index (greater than 10) is much broader than that of BSR metamaterial, demonstrating the broadband property of high refractive index in BSP metamaterial. On the other hand, loss is an important feature for metamaterials, which directly affects their practical applications. In order to evaluate the loss of the proposed metamaterials, we investigate the figure of merit (FOM) that is defined as $\mathrm{Re}(n)/\mathrm{Im}(n)$. Usually, an FOM larger than 10 is typically considered to be low loss of metamaterial.[18] Figure 2(d) gives the FOMs of BSP and BSR metamaterials. It is noted that the FOM of BSP metamaterial is larger than 10 in the frequency range from 0 to 11.6 GHz, verifying the low loss of BSP metamaterial in broadband. Furthermore, we also find that the frequency range of low loss for BSP is much broader than that for BSR. Based on these good performances of BSP metamaterial, we choose it to design lens in the following contents.

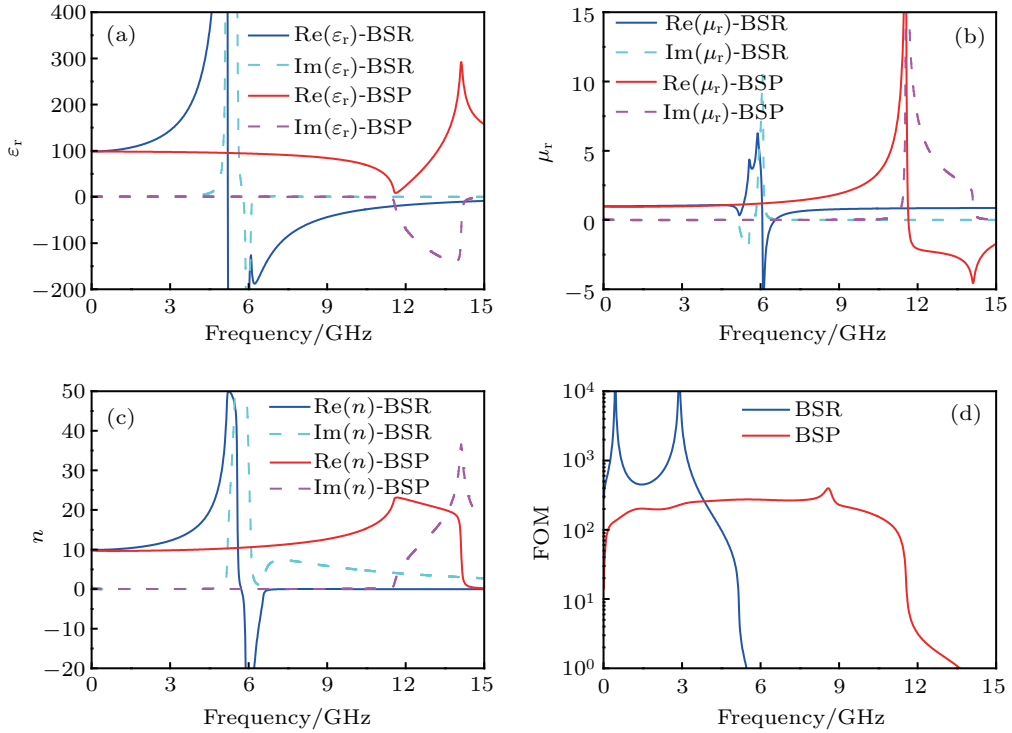


Fig. 2. (color online) Comparison of retrieved effective permittivity, effective permeability, effective refractive index, and figure of merit for the proposed BSP and BSR: (a) Effective permittivity, (b) effective permeability, (c) effective refractive index, and (d) figure of merit.

To investigate the physical mechanism for forming high refractive index in BSP metamaterial, maps of the electric field and surface current distributions on the top and bottom layers are simulated at 5.5 GHz, as shown in Figs. 3(a)–3(b). We clearly see that the electric fields on both top and bottom layers are mainly concentrated at the gaps that are along the y direction [see Fig. 3(a)]. These electric field distributions imply strong capacitive coupling between adjacent patches. Furthermore, the capacitive coupling can be enhanced by reducing the width of the gaps, which further results in high permit-

tivity. Figure 3(b) displays the surface current distributions, from which we observes that the surface currents on top layer are antiparallel to the induced currents on bottom layer. These antiparallel surface currents combined with the displacement currents in dielectric plate will form current loops [see the loop marked as red arrows shown in Fig. 3(b)]. The induced circulating currents can generate magnetic moments that have the same direction as the external magnetic field. As a result, a large paramagnetic effect of the proposed structure is formed, leading to a bigger effective permeability[18] which is almost equal to 1 in non-resonant regime. From the equation $n = \sqrt{\mu_r \varepsilon_r}$, we deduce that the BSP metamaterial should have high effective refractive index because of its high effective permittivity and high effective permeability. As illustrated in Fig. 2(c), it can be seen that the refractive index of the proposed BSP metamaterial monotonically increases from 10 to 23 in the frequency range from 0 to 11.6 GHz, demonstrating its high refractive index characteristic in wideband.

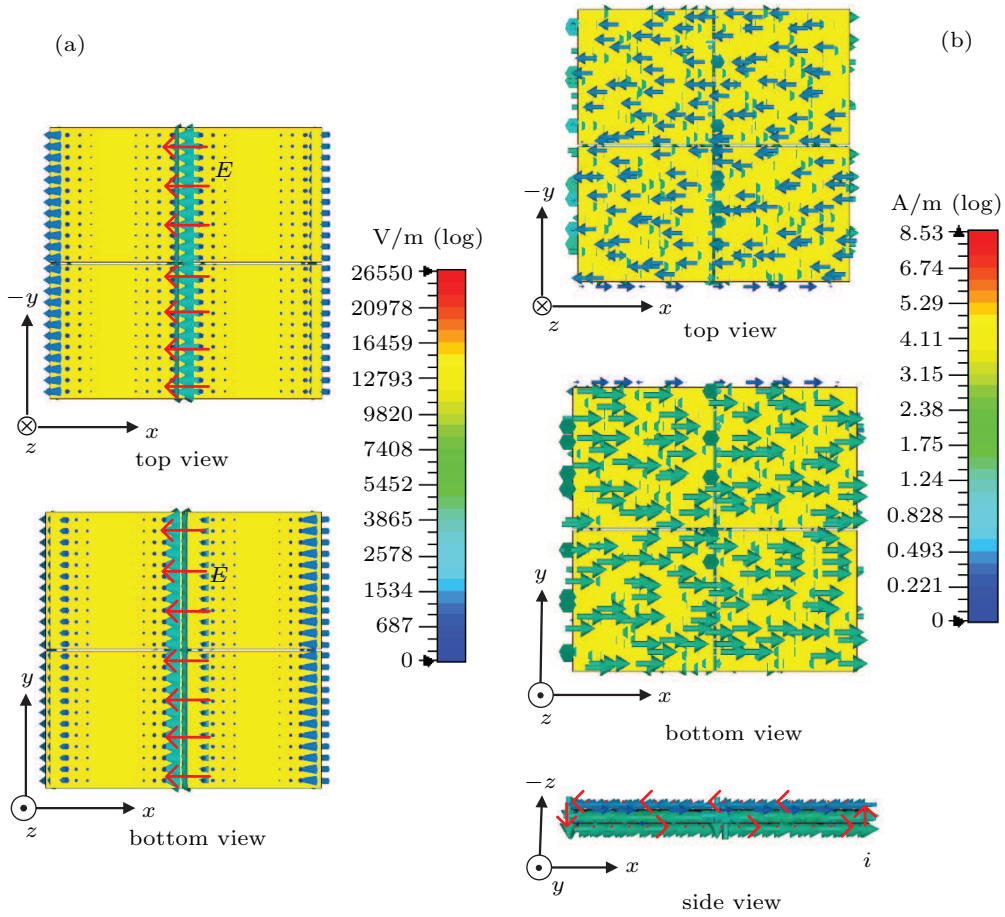


Fig. 3. (color online) Electromagnetic response of BSP at 5.5 GHz: (a) Electric field distributions, and (b) surface current distributions.

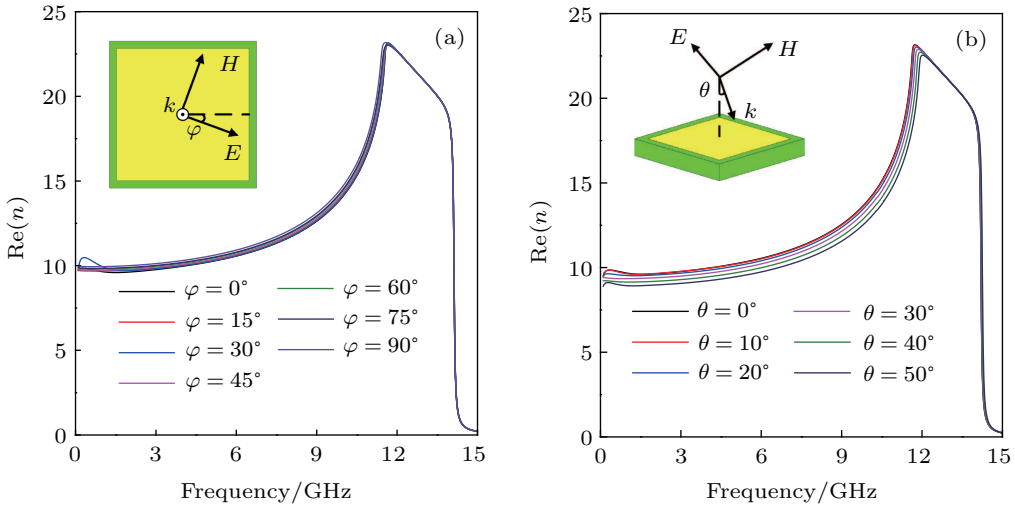


Fig. 4. (color online) Effective refractive index of BSP metamaterial for different polarization and oblique incidence EM waves: (a) The effective refractive index with different polarization direction, and (b) the effective refractive index with varying angle of incidence.

We also investigate the variation of effective index for different polarization direction of exciting field and for oblique incidence. The variation of the effective index with the polarization angle (φ) is plotted in Fig. 4(a). It can be seen that the effective index is insensitive to the polarization direction of exciting field. Figure 4(b) illustrates the refractive index for different incident angles (θ). We note that the real part of refractive index is just slightly decreased when θ increases from 0° to 50°. This insensitive characteristic of effective index for polarization direction and oblique incidence is helpful to design the lens that is used in circular polarization antenna.

3. High-performance lens antenna design

Based on the above investigations of BSP metamaterial, we further design a focusing lens with gradient refractive index distributions satisfying the following equation:

$$n_0 - n(r) = (\sqrt{F^2 + r^2} - F)/T, \tag{1}$$

where F and T denote the focal length and the thickness of lens, respectively. The parameter n_0 is the refractive index at the center of lens, r is the location along the radial direction, and $n(r)$ denotes the refractive index at the location r. According to equation (1), if we increase the difference value of $n_0 - n(r_0)$ (r_0 is the radius of lens), the thickness T of lens can be effectively reduced. To meet this condition, the BSP metamaterial with high refractive index is essential. In addition, two impedance matching layers (IMLs) are symmetrically employed on both sides of lens to decrease the reflection at the air-lens interface (see the coat 1 and coat 2 in Fig. 5). In this case, the lens can be looked as a cascaded circuit consisting of the air, the matching layers, and the core layer. According to the transmission line theory, IMLs can be denoted as

$$Z_{\text{coat 2}} = \sqrt{Z_0 Z_{\text{coat 1}}}, \quad Z_{\text{coat 1}} = \sqrt{Z_{\text{coat 2}} Z_{\text{core}}}, \tag{2}$$

where Z_0, Z_{core}, $Z_{\text{coat 1}}$, and $Z_{\text{coat 2}}$ are impedance of the air, the core layer (core), the first IML (coat 1), and the second IML (coat 2), respectively. From Eq. (2), we can obtain the relationships of the refractive indices between the IMLs and the core layer:

$$n_{\text{coat 1}} = n_{\text{coat 2}}^2, \quad n_{\text{coat 2}} n_{\text{core}} = n_{\text{coat 1}}^2, \tag{3}$$

where $n_{\text{coat 1}}$, $n_{\text{coat 2}}$, and n_{core} are the refractive indices of the coat 1, coat 2, and core, respectively. In order to obtain good impedance matching, the thickness of the IMLs should be approximately equal to 1/4 guide wavelength, namely,

$$t_{\text{coat 1}} = \frac{\lambda_0}{4n'_{\text{coat 1}}}, \quad t_{\text{coat 2}} = \frac{\lambda_0}{4n'_{\text{coat 2}}}, \tag{4}$$

where λ_0 is the wavelength of center frequency in free space,

$$t_{\text{coat 1}} = h_2 + 2t_2 + 2d_2, \quad t_{\text{coat 2}} = h_2 + 2t_2 + 2d_3,$$

$$n'_{\text{coat 1}} \epsilon [n_{\text{coat 1}}(0)\, n_{\text{coat 1}}(r_0)], \quad n'_{\text{coat 2}} \epsilon [n_{\text{coat 2}}(0)\, n_{\text{coat 2}}(r_0)],$$

respectively. The $n_{\text{coat } i}(0)$ and $n_{\text{coat } i}(r_0)$ ($i = 1, 2$) are the refractive indices at the center and the edge of the i matching layer. Due to the usage of the IMLs, equation (1) should be modified into

$$\begin{aligned} & F + n_{\text{core}}(0) t_{\text{core}} + 2n_{\text{coat 1}}(0) t_{\text{coat 1}} + 2n_{\text{coat 2}}(0) t_{\text{coat 2}} \\ = & \sqrt{F^2 + r^2} + n_{\text{core}}(r) t_{\text{core}} + 2n_{\text{coat 1}}(r) t_{\text{coat 1}} \\ & + 2n_{\text{coat 2}}(r) t_{\text{coat 2}}, \end{aligned} \tag{5}$$

where $t_{\text{core}} = h_1 + 2t_1 + 2d_1$. From Eq. (5), a GRIN lens that converts a spherical wave into planar wave can be obtained by tailoring the refractive index distributions (n_{core}, $n_{\text{coat 1}}$, and $n_{\text{coat 2}}$) and designing the thicknesses of each layer (t_{core}, $t_{\text{coat 1}}$, and $t_{\text{coat 2}}$). The designed lens can effectively improve the performance of antenna. Figure 5 shows the schematic of a circular horn antenna loaded with the proposed lens. In order to reduce the longitudinal size of antenna, the lens is placed inside the horn antenna. Figure 6(a) illustrates the refractive

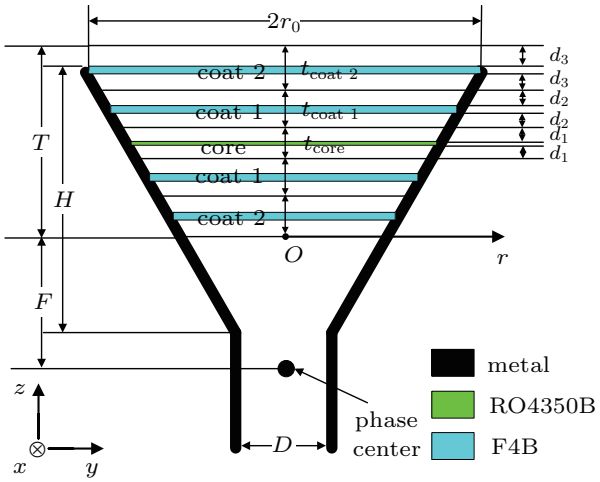


Fig. 5. (color online) The schematic diagram of the lens antenna. The five layers of GRIN lens are designed including one core layer, two coat 1 layers, and two coat 2 layers. The lens antenna dimensions are: $T = 17.688$ mm, $H = 80$ mm, $r_0 = 80$ mm, $D = 46$ mm, $t_{\text{core}} = 1.544$ mm, $t_{\text{coat 1}} = 3.036$ mm, $t_{\text{coat 2}} = 5.036$ mm, $d_1 = 0.5$ mm, $d_2 = 1$ mm, and $d_3 = 2$ mm, respectively. The substrates of the lens are RO4350B ($\varepsilon_{r1} = 3.66$, $\delta_1 = 0.0037$, $h_1 = 0.508$ mm, and $t_1 = 0.018$ mm) and F4B ($\varepsilon_{r2} = 2.2$, $\delta_2 = 0.001$, $h_2 = 1$ mm, and $t_2 = 0.018$ mm). The total thickness of the lens is 17.688 mm ($0.34\lambda_0$).

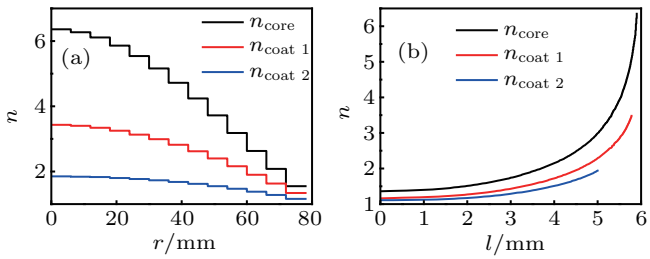


Fig. 6. (color online) The refractive index distributions and realization method: (a) The refractive index distributions for core layer (n_{core}) and the impedance matching layers ($n_{\text{coat 1}}$ and $n_{\text{coat 2}}$), and (b) the relations between length (l) of the square metallic patch for BSP and the refractive index (n_{core}, $n_{\text{coat 1}}$, and $n_{\text{coat 2}}$) at 5.5 GHz.

index distributions of the core layer and the matching layers along the r direction. Figure 6(b) shows the variation of the refractive index of BSP with parameter l (see Fig. 1). According to Figs. 6(a) and 6(b), the GRIN lens can be obtained.

4. Results and discussion

To study the performance of the proposed GRIN lens antenna (LA), we first observe the electric field distributions in the antennas with and without GRIN lens, as shown in Figs. 7(a) and 7(b). It is clearly seen that, for the antenna loaded with lens, the EM wave from phase center is rapidly transformed into a plane wave when it goes through the GRIN lens; whereas for the antenna without lens (CPHA), the EM wave is slowly converted into plane wave when it propagates far away from the antenna. The electric field distribution in LA is helpful to improve the radiation performance of antenna, which is demonstrated by the radiation patterns shown in Fig. 7(c).

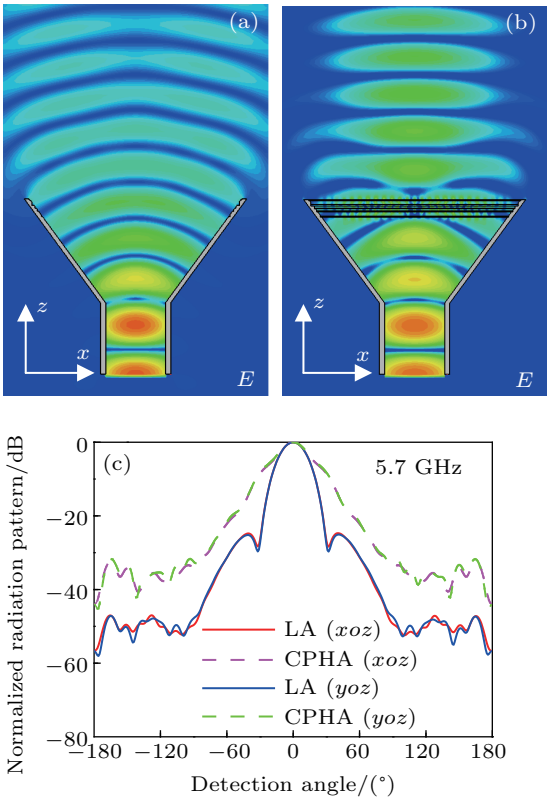


Fig. 7. (color online) Simulated electric-field distributions on the xoz plane of the circular horn (a) without and (b) with GRIN lens at 5.7 GHz; (c) Simulated normalized far-field radiation patterns of CPHA and LA at 5.7 GHz.

To further demonstrate the performance of the proposed antenna, we fabricate the antenna and test its electric parameters including reflection coefficient (S_{11}), normalized radiation pattern, realized gain, and axial ratio (AR). Figure 8(a) presents a photo of the fabricated prototype and figure 8(b) exhibits the comparison of measurement reflection coefficients between LA and CPHA. The reflection coefficient of LA is less than −10 dB in the frequency range from 4 GHz to 7 GHz, which is almost equal to the bandwidth of CPHA, implying that the lens does not deteriorate the stand-wave ratio of antenna.

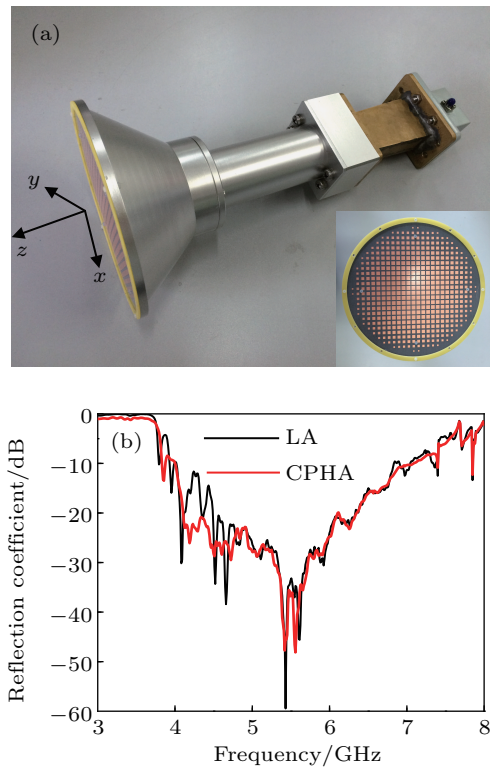


Fig. 8. (color online) (a) The photograph of the lens antenna setup and the inset is the photography of the fabricated lens; (b) Measured reflection coefficients of CPHA and LA.

The normalized far-field radiation patterns of LA and CPHA were measured inside the anechoic chamber. The measurement results at three typical frequencies such as 4.8 GHz, 5.7 GHz, and 6.7 GHz are plotted in Figs. 9(a)–9(c). We see that the main lobe width of LA is much less than that of CPHA. Meanwhile, the side-lobe of LA is less than −20 dB for all observed frequencies. These characteristics verify that the GRIN lens effectively enhances the directivity of antenna. Figure 9(d) illustrates the axial ratios and the gains of LA and CPHA. The 3 dB axial ratio bandwidth of LA is in the frequency range of 4.75 GHz to 6.75 GHz, which is less than that of CPHA. By carefully observing Fig. 9(d), we find that the axial ratio of LA is deteriorated in the frequency regions from 4.5 GHz to 4.8 GHz and from 6.7 GHz to 7.0 GHz. Accordingly, the reflection coefficients of LA in the two frequency regions are larger than that of CPHA, which can be seen from Fig. 8(b). Therefore, we deduce that the reduction of axial ratio bandwidth of LA may be affected by its large reflection coefficient. From this point of view, the axial ratio bandwidth of LA can be further extended by increasing the number of impedance matching layer. From Fig. 9(d), we also see that the gain of LA shows an average increase of 3.4 dB (between 1.45 dB and 5.18 dB), over a frequency range from 4.75 GHz to 6.75 GHz.

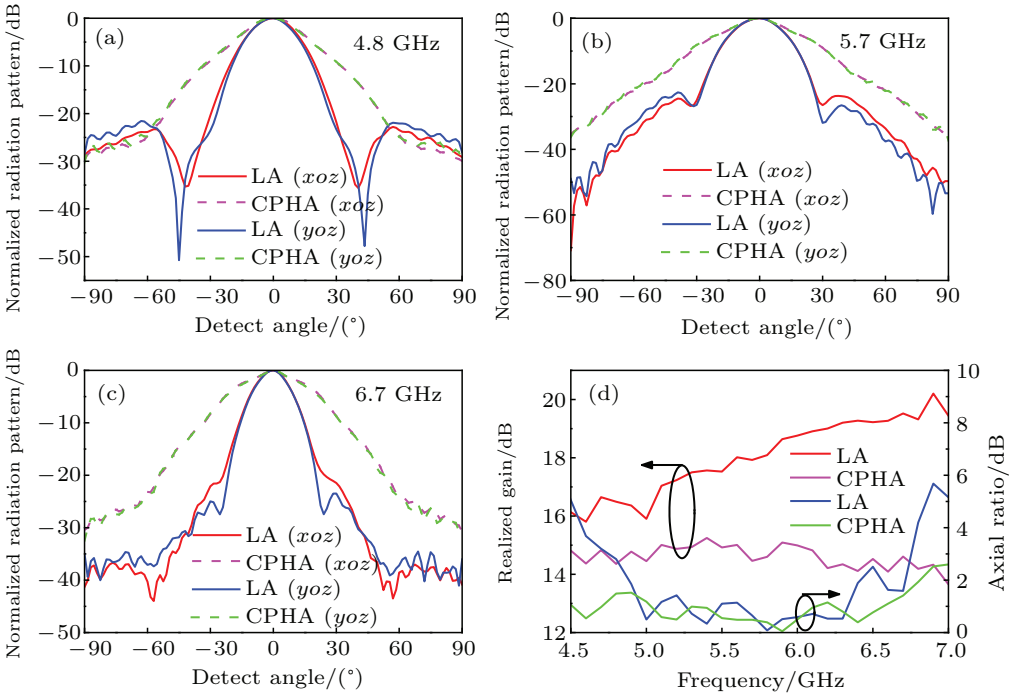


Fig. 9. (color online) Measured normalized far-field radiation patterns of CPHA and LA for different operating frequencies: (a) 4.8 GHz, (b) 5.7 GHz, and (c) 6.7 GHz; (d) Measured axial ratios and realized gains of CPHA and LA.

In order to evaluate the whole performance of the proposed antenna, we also investigate the antenna aperture efficiency. According to Ref. [13], the antenna efficiency at a certain frequency can be calculated by $\eta = G_{\mathrm{m}}/D_{\mathrm{m}}$, where G_{m} is gain and D_{m} that is defined as $D_{\mathrm{m}} = 4\pi A/\lambda^2$ (A is the aperture area of the antenna and λ is the wavelength of operation frequency) is the maximum directivity. Then the calculated results show that the minimum antenna efficiency is 59% at 5 GHz and the maximum is 77% at 5.6 GHz. In all, the performance of LA is greatly improved except the slight reduction of axial ratio bandwidth.

In Table 1, we present a comparison between the proposed LA and the other reported works in Refs. [12], [14], and [15]. The comparison shows that the proposed lens has the greatest variation of the refractive index and hence has the thinnest thickness. Moreover, the proposed lens can effectively reduce the size of the antenna while improving the antenna performance.

Table 1. Comparison with other works.

LA	[12]	[14]	[15]	This work
f_0/GHz	10	10	5	5.75
Polarization	linear	circular	linear	circular
Refractive	1.1–2.1	1.2–1.5	1.1–1.7	1.1–6.4
$H/(2r_0)$	0.63	1.01	0.91	0.5
Thickness/λ_{g}	0.9	1.33	0.8	0.34
Bandwidth/%	40.8 (S_{11})	> 40 (AR)	> 66.7 (S_{11})	54.6 (S_{11}) 34.8 (AR)

5. Conclusion

A novel circular polarization LA operating at C band with improved radiation performance has been numerically and experimentally demonstrated by an HRM. The HRM is designed on BSP elements which provide a powerful solution to synchronously increase the effective permittivity and the effective permeability in broadband, resulting in the enhancement of refractive index. Based on the proposed HRM, a GRIN lens with thin thickness ($0.34\lambda_0$) is designed. By locating the lens inside a circular polarization horn antenna, the radiation performance of antenna is dramatically improved. The simulation and measurement results show that the 3 dB axial ratio bandwidth of the LA is in the frequency range from 4.75 GHz to 6.75 GHz (the relative bandwidth is 34.8%). The antenna gain is significantly increased by a mean value of 3.4 dB, over the operation frequency range, and the competitive aperture efficiency is better than 59%.

References

[1] Kock W E 1948 *Bell Labs Tech. J.* **27** 58

[2] Kock W E 1946 *Proc. IRE* **34** 828
[3] Greegor R B, Parazzoli C, Nielse J, Thompson M A, Tanielian M H and Smith D R 2005 *Appl. Phys. Lett.* **87** 091114
[4] Yu N F, Genevet P, Kats M A, Aieta F, Tetienne J P, Capasso F and Gaburro Z 2011 *Science* **334** 333
[5] Li H P, Wang G M, Liang J G and Gao X J 2016 *Prog. Electromag. Res.* **155** 115
[6] Wan X, Jia S L, Cui T J and Zhao Y J 2016 *Sci. Rep.* **6** 25639
[7] Pfeiffer C, Emani N K, Shaltout A M, Boltasseva A, Shalaev V M and Grbic A 2014 *Nano Lett.* **14** 2491
[8] Wu R Y, Li Y B, Wu W, Shi C B and Cui T J 2017 *IEEE Trans. Anten. Propag.* **65** 3481
[9] Smith D R, Mock J J, Starr A F and Schurig D 2005 *Phys. Rev. E* **71** 036609
[10] Ma H F and Cui T J 2010 *Nat. Commun.* **1** 124
[11] Mei Z L, Bai J, Niu T M and Cui T J 2012 *IEEE Trans. Anten. Propag.* **60** 398
[12] Chen X, Ma H F, Zou X Y, Jiang X W and Cui J T 2011 *J. Appl. Phys.* **110** 044904
[13] Xu H X, Wang G M, Tao Z and Cui T J 2015 *Sci. Rep.* **4** 5744
[14] Meng F Y, Liu R Z, Zhang K, Erni D, Wu Q, Sun L and Li L W 2013 *Prog. Electromag. Res.* **141** 17
[15] Qi M Q, Tang W X, Ma H F, Pan B C, Tao Z, Sun Y Z and Cui T J 2015 *Sci. Rep.* **5** 9113
[16] Ma H F, Chen X, Xu H S, Yang X M, Jiang W X and Cui T J 2009 *Appl. Phys. Lett.* **95** 094107
[17] Tao Z, Jiang W X, Ma H F, Cui T J 2018 *IEEE Trans. Anten. Propag.* **66** 16
[18] Shin J, Shen J T and Fan S 2009 *Phys. Rev. Lett.* **102** 093903
[19] Choi M, Lee S H, Kim Y, Kang S B, Shin J, Kwak M H, Kang K Y, Lee Y H, Park N and Min B A 2011 *Nature* **470** 369
[20] Liu Z X, Zhang C, Sun S, Yi N B, Gao Y S, Song Q H and Xiao S M 2015 *Opt. Mater. Exp.* **5** 1949
[21] Singh L, Singh R and Zhang W L 2017 *J. Appl. Phys.* **121** 233103
[22] Chen X D, Grzegorczyk T M, Wu B I, Pacheco J and Kong J A 2004 *Phys. Rev. E* **70** 016608